DETERMINATION OF FLIGHT STABILITY COEFFICIENTS USING A FINITE ELEMENT CFD

Charles R. O'Neill
Mechanical and Aerospace Engineering
Oklahoma State University
Stillwater, OK 74077

Abstract

A 3D finite element Euler CFD is used to determine forces and moments acting on a low speed aircraft. STARS determines pressures acting on a surface. The surface pressures are integrated to yield forces and moments. Results are compared with static stability theory. Problems with low speed analysis with Euler solvers are discussed.

Nomenclature

GMA = Generic Modular Airplane
CFD = Computational Fluid Dynamics
STARS = STtructural Analysis RoutineS
C_p = Pressure Coefficient
C_L = Lift Coefficient
C_D = Drag Coefficient
C_m = Pitch Moment Coefficient
C_l = Roll Moment Coefficient
C_n = Yaw Moment Coefficient
C_Y = Side Force Coefficient
α = Angle of Attack
β = Sideslip Angle
M = Mach Number

Introduction

Determination of aircraft stability coefficients has traditionally been relegated to the wind tunnel or estimates from basic theory. Neither of these methods is attractive from the standpoint of aircraft design. In contrast, CFD offers reasonable results from arbitrary geometries.

Wind tunnel tests require both the construction of a model and an adequate test facility. Additionally, the lag time between the paper design and the wind tunnel results can be considerable. Furthermore, any configuration change requires a change of the test model.

The traditional method of determining stability coefficients during aircraft design has been from stability theory or an estimation source such as the USAF DATCOM. Simple theory is only accurate for preliminary design or relationships between the overall aircraft geometry and stability[1]. Estimation sources such as the USAF DATCOM are based on fitted data and are thus only valid for certain conditions. In the end, any data obtained from a complied source is only an estimate.

CFD offers a more direct approach to finding stability coefficients. Integration of surface pressures along the body gives the resulting aerodynamic forces and moments. In general, the most complicated geometry can be solved with the proper selection of a CFD method. Finding an efficient, solvable and accurate method of determining pressures is a problem. In the past, solutions to full aircraft configurations has been a problematic due to limitations in computing speed, storage space and geometry definitions. CFD solutions to arbitrary aerodynamic problems are now available due to increases in computer power. CFD allows for analysis of nearly any geometry or flight condition. Using CFD for determining forces and moments is common. However, most low Mach number aircraft are modeled with panel methods and not finite element Euler methods. Park[2] used a panel method to determine pitch stability coefficients of a swept wing aircraft at Mach 0.6. The results compared favorably to experimental data below 6 degrees. Pesonen[3] used a panel method combined with a finite element viscous solver to determine the forces and moments on two low Mach number finite wings. The results closely matched experimental data. Panel methods are not applicable to higher speed flows due to assumptions failing at for large disturbances.

The majority of studies for determining stability coefficients using Euler methods are at least high speed subsonic (M>0.6). Prabhu[4] determined the moments and forces on the X-33 using a finite element Euler CFD. The calculations were made at Mach 6.0 and above. This study gives evidence that Euler solvers are capable of determining aerodynamic forces and moments within the CFD's assumptions. To obtain these forces, the computational domain required from 6.5 to 8 million elements. Clearly, finite element solvers are capable of excellent solution given enough computer power.

One method of increasing the solution accuracy of a finite element method is to remesh the elements. Remeshing involves changing the element spacing to account for the flow gradients. This is determined by an iterative method of solving an initial grid and updating the elements with the solution. Not surprisingly, Shapiro[5] found that remeshing better than an overall fine grid. One disadvantage of remeshing is the added complexity to change the element distribution in a manner that reflects the flow patterns without distorting the next resulting

solution. CFD literature contains countless other ingenious methods of creating better results from less powerful computers.

The goal of this study is to determine the static stability coefficients for a generic modular aircraft. A finite element Euler solver will be used. The results will be verified with simple static stability theory.

Computational Methods

STARS is a 3D finite element Euler CFD developed by NASA. STARS is capable of unsteady, vibration and thermal solutions; however, this project will only require the steady solver[5]. Geometries in STARS are defined by a series of curves and surfaces. These are defined in a .sur file and are run through *surface* which places elements along the surface of the body. Next, v*olume* fills in the computational domain between the surfaces and the outer background with triangular elements. *Setbnd* configures the boundaries for the solver. S*teady* contains the Euler solver. Postprocessing was performed with *glplot*.

An AMD Athlon 800 MHz PC was used in for all computer computations. A total of 128Mbytes of RAM was available; however, the operating system had to reside inside of the 128 Mbytes so the true amount available was somewhat less. The steady solver for the 1.2 million element GMA required 3.3 hours to converge with 600 iteration per flight condition.

GMA

The GMA is based on the OSU Flight Factory's Design Build and Fly competition aircraft. The general configuration of the Flight Factory aircraft is preserved in the GMA geometry except for the wing. The Flight Factory aircraft was a biplane configuration whereas the GMA is a monoplane. The Flight Factory aircraft also used a highly cambered Selig airfoil; however, for a computational reason as discussed in the results below, the GMA uses the NACA 0009 (Appendix B) for all airfoil surfaces. The wing is un-twisted and constant chord of 12 inches with a wingspan of 120 inches. The horizontal has a chord of 13 inches and is set at negative 3 degrees angle of incidence with respect to the wing. The GMA cowling, which tapers from the firewall forward, is simplified geometrically from the Flight Factory aircraft. The Cartesian coordinate origin as defined in the CFD geometry is at the bottom center of the firewall.

The GMA was defined in STARS with by defining curves and surfaces. Parameters describing the characteristic shape and location of the fuselage, wing, horizontal stabilizer and vertical stabilizer were input into an Excel spreadsheet. This spreadsheet was designed to define points, curves and surfaces compatible with the STARS surface input file. The curves defining the GMA are shown in Figure 1 in Appendix F.

The GMA volume mesh consists of almost 1.2 million elements of which 72000 are on the aircraft's surface. Element line sources were added to high gradient to increase the number of areas surfaces elements. These extra surface elements are seen most vividly on the leading edge of the wing. The surface elements of the GMA are shown in Figure 2.

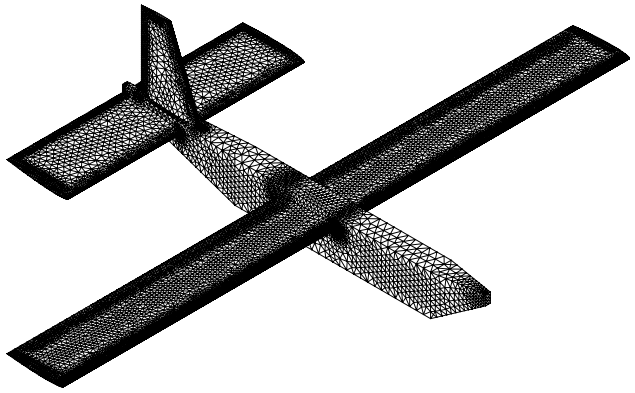

Fig. 1 GMA Surface Elements

An Excel spreadsheet was created to automatically create the input geometry data of the GMA. General parameters such as wingspan and airfoil shape are automatically configured into the proper .sur file. The fuselage length, width, height and taper can be changed by changing only the desired parameter. With minor modifications, this spreadsheet could generate the .sur file for any wing or stabilizer with arbitrary airfoil sections, wing twist, taper, sweep and dihedral.

Results and Discussion

This project consisted of two parts. The first was to learn how to configure the input geometry and element generators in STARS to accurately model the airfoil. The second part was to apply the lessons to the GMA and determine the stability coefficients.

Pressure distributions along the chord were computed from the STARS output files and the results are verified with a 2-D Smith-Hess panel method and *Theory of Wing Sections*[7] where possible. Cross sectional cuts of the wing pressure distributions are made at y=20 *in*. This outboard location prevents interference problems with the fuselage while staying away from the reduced lift distribution of the wing tip.

At α=0 and β=0 (**Fig. 2**), the pressure distribution along the wing chord matches the 2-D panel method and *Theory Of Wing Sections* (TOWS) data. It was noticed that the upper and lower pressure distributions do not match even though the wing section is at zero angle of attack. By looking at a 3-D color pressure distribution plot, it was found that the upper surface pressure distribution was being detrimentally affected by the fuselage. The fuselage below the wing acts as a symmetry plane while the lack of fuselage area above the wing makes the pressure coefficient go to the free stream value at the fuselage.

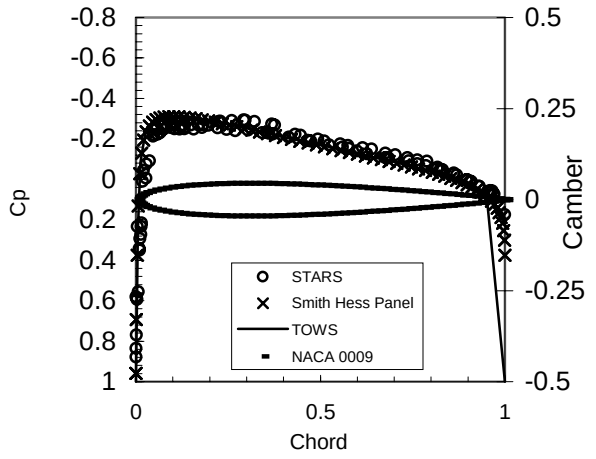

Fig. 2 NACA 0009 Pressure distribution α=0 β=0

At higher angles of attack, the solution at the leading edge became progressively worse. The solver was unable to accelerate the flow fast enough around the leading edge of the wing. Additionally, the pressure peak near the leading edge was being attenuated due to the solver dissipation. Dissipation is required to prevent spurious spikes in the data.; however in this case it is hurting the accuracy of the solution.

A wing utilizing the Selig 4083 airfoil (Appendix A) was tested. The Selig 4083 is a highly cambered airfoil. The camber created problems later. A test with the same leading edge grid spacing as in the 3D case was not consistent with the Smith-Hess panel method. A smaller grid spacing with at the leading edge helped, but the errors in the pressure distribution were 20% or more at the pressure peak near the leading edge In an attempt to fix this pressure peak problem, a 2-D Euler CFD solver was used with the Selig 4083 airfoil. This 2D solution will have no disturbances from vortices due to lift or the fuselage. Additionally, because the solver is 2D, the resulting pressure distribution should match the Smith-Hess result. An element spacing equal to the spacing of the 3D wing was used initially, but the resulting pressure distribution closely matched the incorrect 3D case. The leading edge elements were made smaller by a factor of more than two to obtain a better result. While the results are better, the solution is not exactly matched with the Smith-Hess panel method. This is discouraging. To obtain a decent pressure distribution for the Selig 4083, the number of elements must be high. If the element spacing used in the 2D case were transferred to the 3D case, the number of elements would be well over 2 million. The original 3D case was at the limit of the RAM installed in the computer. Even worse, the time required for a solution is increased by a factor of at least three. From a computational standpoint, the Selig 4083 requires much more computational power to solve than the NACA 0009. Due to the added computational problems with the Selig airfoil, a decision was made to only consider the stability coefficients for the GMA case with the NACA 0009 airfoil.

Forces and moments were determined by integrating the pressure distributions calculated by STARS. Tabulated results are given in Table 1 of Appendix D. Non-dimensional forms are given in Table 2 of Appendix D and plotted in Figures 1 through 5 in Appendix E. A drag polar is included as Figure 6 in Appendix E. Estimated stability coefficients were calculated from theory and are given in Appendix C. Three dimensional pressure plots are given in Appendix G.

Figure 1 plots the lift coefficient versus angle of attack. The lift coefficient versus angle of attack is linear with a slope of 0.11 per degree with a zero lift angle of attack of 1 degree. Because the NACA 0009 airfoil has zero lift at an angle of attack of 0 degrees, the lowered lift line is due to the horizontal stabilizer. The horizontal is creating a downward lift coefficient of 0.12 at zero angle of attack. This is expected due to the 3 degrees angle of incidence in the horizontal. Theory did not account for the stabilizer reducing the effective lift. STARS output a lift slope curve 20% higher than theory predicted. This could be in part to lift from other surfaces.

Drag coefficient versus angle of attack is plotted in Figure 2. As predicted by theory, the drag curve is linear with respect to lift coefficient squared. This square relationship indicates induced drag. The CFD solver must be correctly accounting for trailing vortices since induced drag is present.

Pitching moment versus angle of attack is plotted in Figure 3. As expected for a stable aircraft, the pitching moment slope is negative with a value of –0.072 per degree. Thus, the GMA is trimmed to fly at 4.2 degrees, which is a 0.35 lift coefficient. Theory estimated a moment slope of –0.062 per degree.

In the lateral axes, roll moment and yaw moment were calculated. Roll moment versus a sideslip angle is plotted in Figure 4. The roll moment is linear with respect to sideslip angle and has a slope of –0.0012 per degree. Theory didn't predict a roll moment due to the wing having zero dihedral. The fuselage and vertical stabilizer are creating desirable roll moments. Positive roll moments are expected with high wing aircraft. Yaw moment versus sideslip angle is plotted in Figure 5. The yaw moment slope is 0.0068 per degree. Theory predicted 0.0029 per degree. The aircraft is statically stable in the lateral axes.

While the objective of determining stability coefficients was met, problems in determining the pressure distributions prevented the current GMA configuration from allowing arbitrary airfoil geometries. STARS may not be the ideal CFD solver for low speed aerodynamics. STARS was not designed specifically for very low Mach numbers, instead it seems tailored for higher subsonic to supersonic flows. The dissipation used in STARS for convergence seems to favor high subsonic to supersonic flows flows. Because the GMA is a low subsonic aircraft, the boundary layers will extend further from the body.

Because STARS is based on an Euler solution and not a general Navier-Stokes solution, the flow solution does not account for boundary layer effects. The computations required to generate a Navier-Stokes general solution would be expected to vastly outnumber that of an Euler solution. Low Mach number analysis is difficult due to the magnitudes of the parameters. Changes in pressures are low due to a low dynamic pressure. Special care must be taken in low speed computations to keep the pressure gradients smooth. Surface pressures are affected even by poorly defined gradients far from the body. This requires many elements to be generated. More elements require more iterations to convergence and are slower per iteration.

Conclusions

Stability coefficients for the GMA were found for angles of attack ranging from –2.5 degrees to 10 degrees and sideslip angles from 0 to 10 degrees. The computationally determined stability coefficients were similar to those calculated from theory. As expected, the GMA exhibited stable characteristics in the static coefficients.

It was found that low subsonic flows are difficult to solve. This is due in part to the low magnitudes of pressures and velocities dealt with in subsonic flows. Additionally, the number of elements required for accurate solutions are immense and increase drastically the computational time to converge to a solution. Finite element methods require vast amounts of memory especially for low speed subsonic flows. While 3D finite element Euler solvers are impressive, low subsonic flows are difficult to properly model. Panel methods, while no doubt less impressive from a computational standpoint, are probably better for determining stability coefficients for low subsonic aircraft.

Some airfoils are more difficult to accurately model due to the aerodynamic interactions between the flow solver and the airfoil geometry. The Selig 4083 was found unsuitable for the wing airfoil section due to problems with creating sufficient elements to accurately model the flow around the leading edge. This problem with the leading edge vividly provides a reason to verify computational solutions. Without investigation, the lowered pressure coefficients for the Selig airfoil would have been incorrectly attributed to only three-dimensional effects.

In general, CFD solvers are capable of analyizing most aerodynamic problems. While the solutions are capable of corresponding nearly perfectly with experimental results, the output quality is vastly dependent on the input quality.

References

1. Nelson, R. C., *Flight Stability and Automatic Control*, McGraw-Hill, Boston.
2. Park, M.A., et. al, "Determination of Stability and Control Derivatives Using Computational Fluid Dynamics and Automatic Differentiation", AIAA Paper 99-3136, June 1999.
3. Pesonen, U. J., Agarwal, R. K., and Laine, S., "Fast and Robust Viscous/Inviscid Interaction Code for Wing Flowfield Calculations," *Journal of Aircraft*, Vol. 37, No. 4, 2000, pp. 730-733.
4. Prabhu, R. K., "An Inviscid Computational Study of the X-33 Configuration at Hypersonic Speeds," NASA CR 209366, July 1999.
5. Shapiro, R. A., Cartesian Grid Finite Element Solutions to the Euler Equations,´AIAA Paper 87-0559, Jan. 1987.
6. Gupta, K. K., "STARS-An Integrated, Multidisciplinary, Finite-Element, Structural, Fluids, Aeroelastic, and Aeroservoelastic Analysis Computer Program," NASA TM 4795, May 1997.
7. Abbott, I. H., and von Doenhoff, A. E., *Theory of Wing Sections*, Dover Publishing, New York.

.

Appendix A:
Selig 4083 Airfoil Data

Chord	Camber				
1.000000	.000000	.273781	.073131	.259356	-.006996
.994150	.001852	.257939	.072829	.275849	-.006247
.983322	.004945	.242126	.072310	.292347	-.005492
.970157	.007802	.226398	.071558	.308848	-.004736
.955232	.010525	.210803	.070550	.325347	-.003981
.939635	.013129	.195332	.069258	.341839	-.003231
.923780	.015599	.179903	.067652	.358322	-.002489
.907762	.017971	.164491	.065738	.374801	-.001757
.891681	.020252	.149205	.063520	.391280	-.001037
.875547	.022454	.134123	.060974	.407754	-.000329
.859350	.024594	.119233	.058066	.424216	.000363
.843113	.026683	.104509	.054762	.440665	.001037
.826873	.028720	.090058	.051062	.457111	.001687
.810624	.030705	.076042	.046951	.473564	.002317
.794338	.032647	.062423	.042350	.490023	.002927
.778029	.034555	.049442	.037305	.506480	.003518
.761724	.036425	.037392	.031831	.522931	.004087
.745415	.038257	.026697	.026078	.539381	.004634
.729086	.040055	.017844	.020389	.555836	.005160
.712736	.041827	.011304	.015347	.572302	.005667
.696377	.043571	.007133	.011446	.588776	.006156
.680022	.045289	.004231	.008060	.605244	.006626
.663675	.046977	.002180	.005188	.621674	.007070
.647329	.048634	.000851	.002987	.638039	.007472
.630968	.050262	.000151	.001148	.654338	.007808
.614591	.051865	.000002	-.000612	.670592	.008065
.598214	.053444	.000399	-.002371	.686828	.008233
.581850	.054993	.001425	-.003977	.703067	.008308
.565492	.056511	.003271	-.005284	.719328	.008293
.549129	.057996	.006115	-.006433	.735618	.008197
.532768	.059448	.010086	-.007678	.751939	.008029
.516422	.060862	.015564	-.008943	.768289	.007798
.500094	.062232	.023562	-.010157	.784662	.007512
.483769	.063553	.035293	-.011292	.801046	.007177
.467438	.064825	.049212	-.012079	.817418	.006795
.451115	.066048	.064401	-.012521	.833776	.006363
.434819	.067210	.080070	-.012680	.850153	.005879
.418556	.068300	.095967	-.012617	.866552	.005351
.402321	.069310	.112060	-.012391	.882922	.004781
.386109	.070229	.128248	-.012040	.899281	.004161
.369921	.071048	.144498	-.011591	.915696	.003495
.353758	.071759	.160806	-.011061	.932116	.002803
.337626	.072349	.177169	-.010471	.948456	.002082
.321544	.072803	.193570	-.009835	.964660	.001393
.305543	.073102	.209985	-.009163	.980280	.000789
.289635	.073219	.226417	-.008461	.993529	.000271
		.242874	-.007736	1.000000	.000000

Appendix B:
NACA 0009 Airfoil Data

Chord	Camber				
		.266276	.044915	.266276	-.044915
1.000000	.000000	.250174	.044663	.282373	-.045063
.992588	.000977	.234093	.044308	.298486	-.045109
.978431	.002727	.218057	.043835	.314631	-.045063
.962932	.004519	.202046	.043231	.330794	-.044937
.946984	.006252	.186062	.042490	.346965	-.044734
.930890	.007916	.170138	.041598	.363143	-.044460
.914755	.009526	.154273	.040535	.379330	-.044117
.898598	.011088	.138473	.039283	.395527	-.043709
.882422	.012606	.122778	.037819	.411732	-.043241
.866228	.014086	.107202	.036110	.427944	-.042716
.850019	.015533	.091745	.034125	.444162	-.042138
.833798	.016950	.076471	.031840	.460383	-.041511
.817571	.018340	.061545	.029225	.476607	-.040835
.801341	.019703	.047280	.026246	.492833	-.040113
.785109	.021040	.034392	.022919	.509062	-.039347
.768877	.022350	.023705	.019346	.525293	-.038538
.752645	.023634	.015757	.015817	.541527	-.037689
.736410	.024889	.010145	.012508	.557764	-.036802
.720173	.026117	.006356	.009616	.574002	-.035878
.703932	.027318	.003720	.007082	.590242	-.034920
.687689	.028491	.001851	.004763	.606482	-.033927
.671446	.029638	.000663	.002678	.622722	-.032902
.655203	.030756	.000076	.000856	.638962	-.031844
.638962	.031844	.000076	-.000856	.655203	-.030756
.622721	.032902	.000663	-.002678	.671446	-.029638
.606482	.033927	.001851	-.004763	.687689	-.028491
.590242	.034920	.003720	-.007082	.703932	-.027318
.574002	.035878	.006356	-.009616	.720173	-.026117
.557763	.036802	.010145	-.012508	.736410	-.024889
.541527	.037689	.015757	-.015817	.752645	-.023634
.525293	.038538	.023705	-.019346	.768877	-.022350
.509062	.039347	.034392	-.022919	.785110	-.021040
.492833	.040113	.047281	-.026246	.801341	-.019703
.476607	.040835	.061545	-.029225	.817571	-.018340
.460383	.041511	.076471	-.031840	.833798	-.016950
.444162	.042138	.091745	-.034125	.850019	-.015533
.427944	.042716	.107202	-.036110	.866228	-.014086
.411732	.043241	.122778	-.037819	.882422	-.012606
.395527	.043709	.138473	-.039283	.898598	-.011088
.379330	.044117	.154273	-.040535	.914755	-.009526
.363143	.044460	.170138	-.041598	.930890	-.007916
.346965	.044734	.186062	-.042490	.946984	-.006252
.330794	.044937	.202046	-.043231	.962932	-.004519
.314630	.045063	.218057	-.043835	.978431	-.002727
.298486	.045109	.234093	-.044308	.992588	-.000977
.282373	.045063	.250174	-.044663	1.000000	.000000

Appendix C:
Coefficients from Theory

Longitudinal Stability:

Wing: Selig 4083

$$C_{m_{0w}} = C_{m_{ac}} = 0$$

$$C_{l_0} = 0$$

$$AR = 10$$

$$C_{L_\alpha} = \frac{2\pi}{1+\frac{2\pi}{10\pi}} = 5.24$$

$$C_{L_\alpha} = 0.091$$

Horizontal Stabilizer:

$$i_t = -3.0^{\deg}$$

$$V_H = 1.29$$

$$AR = 3.85$$

$$C_{L_\alpha} = 4.14^{1/rad}$$

$$\frac{d\varepsilon}{d\alpha} = 0.33$$

$$C_{m_0} = (1.29)(4.14)(0.052) = 0.279$$

$$C_{m_\alpha} = -(1.29)(4.14)(1-0.33) = -0.062^{1/\deg}$$

Total:

$$C_m = 0.279$$

$$C_{m_\alpha} = -0.062^{1/\deg}$$

Lateral Stability:

$$AR_v = 1.7$$

$$C_{L_\alpha} = 2.9$$

$$\eta\left(1+\frac{d\sigma}{d\beta}\right) = 1.38$$

$$C_{n\beta} = V_v \eta C_{L_\alpha}\left(1+\frac{d\sigma}{d\beta}\right) = \frac{(57)(150)}{120^2 \cdot 12}(2.9)(1.38) = 0.2^{1/rad}$$

$$C_{n\beta} = 0.0035^{1/\deg}$$

$$C_{n\beta_{wing-fuselage}} = -0.0006 \approx 0$$

$$C_{n\beta} = 0.0029$$

$$C_{l\beta} \approx 0 \qquad no \quad dihedral$$

Appendix D:
Tabulated Force and Moment Results

α	β	Force x	Force y	Force z	Roll Moment	Pitch Moment	Yaw Moment
-2.5000	0.0000	14.1620	-0.5924	-561.2579	103.6564	20874.5700	-21.9867
0.0000	0.0000	26.5173	-0.3823	-165.7867	73.0062	9158.1150	-11.1536
2.5000	0.0000	9.6632	-0.4704	250.5501	74.2941	-3458.1140	-35.6074
5.0000	0.0000	-6.3915	-0.2954	639.2454	63.2464	-15702.2700	-40.7742
10.0000	0.0000	-62.3253	0.1894	1414.7650	28.0723	-39913.1100	-448.2042
0.0000	0.0000	26.5173	-0.3823	-165.7867	73.0062	9158.1150	-11.1536
0.0000	5.0000	15.4714	102.7728	-160.7993	-939.9965	8690.4050	3515.3880
0.0000	10.0000	12.3262	205.7954	-157.5735	-1955.9420	8457.1700	7047.6370

Table 1: Raw forces and moment

α	β	CD	CY	CL	Cl	Cm	Cn
-2.5000	0.0000	0.0268	-0.0039	-0.3890	0.0006	0.4610	-0.0002
0.0000	0.0000	0.0184	-0.0025	-0.1151	0.0004	0.3093	-0.0001
2.5000	0.0000	0.0143	-0.0031	0.1735	0.0004	0.1334	-0.0003
5.0000	0.0000	0.0343	-0.0020	0.4426	0.0004	-0.0578	-0.0003
10.0000	0.0000	0.1280	0.0013	0.9751	0.0002	-0.4267	-0.0026
0.0000	0.0000	0.0184	-0.0025	-0.1151	0.0004	0.3093	-0.0001
0.0000	5.0000	0.0107	0.6852	-0.1117	-0.0054	0.2889	0.0340
0.0000	10.0000	0.0086	1.3720	-0.1094	-0.0113	0.2797	0.0682

Table 2: Non-Dimensional forces and Moments

Appendix E:
Force and Moment Plots

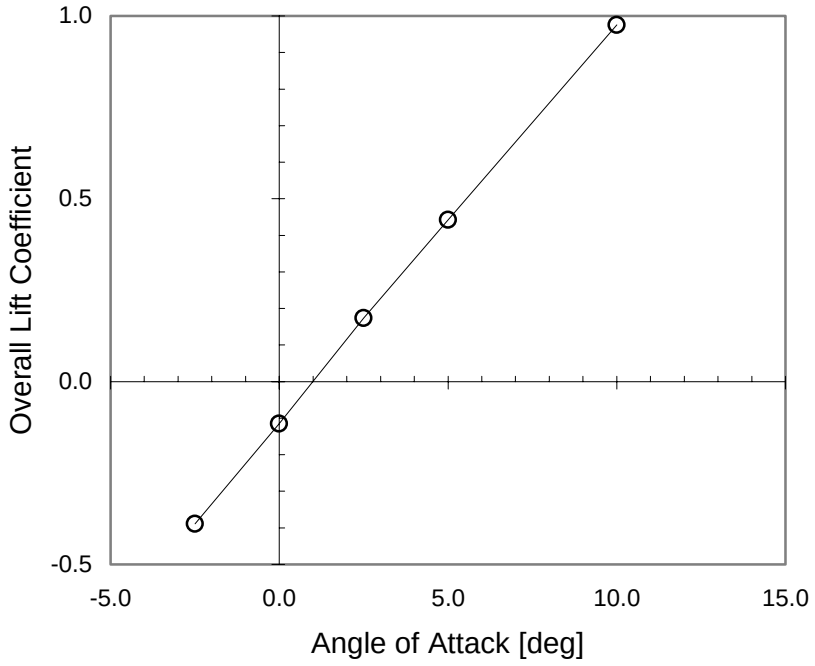

Figure 7: Lift Coefficient versus Angle of Attack

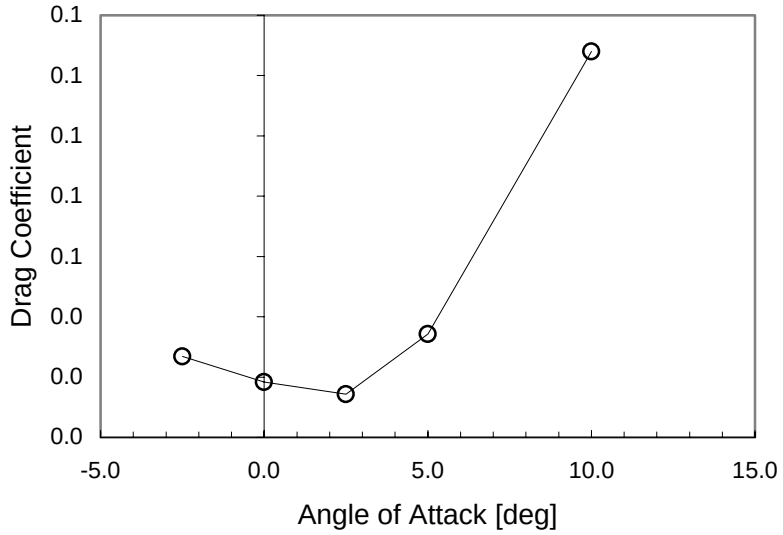

Figure 2: Drag Coefficient versus Angle of Attack

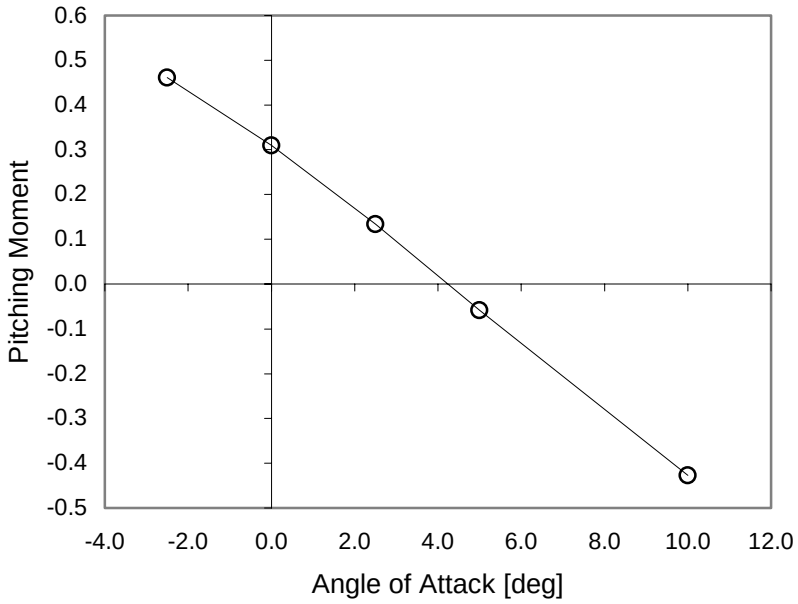

Figure 3: Pitching Moment versus Angle of Attack

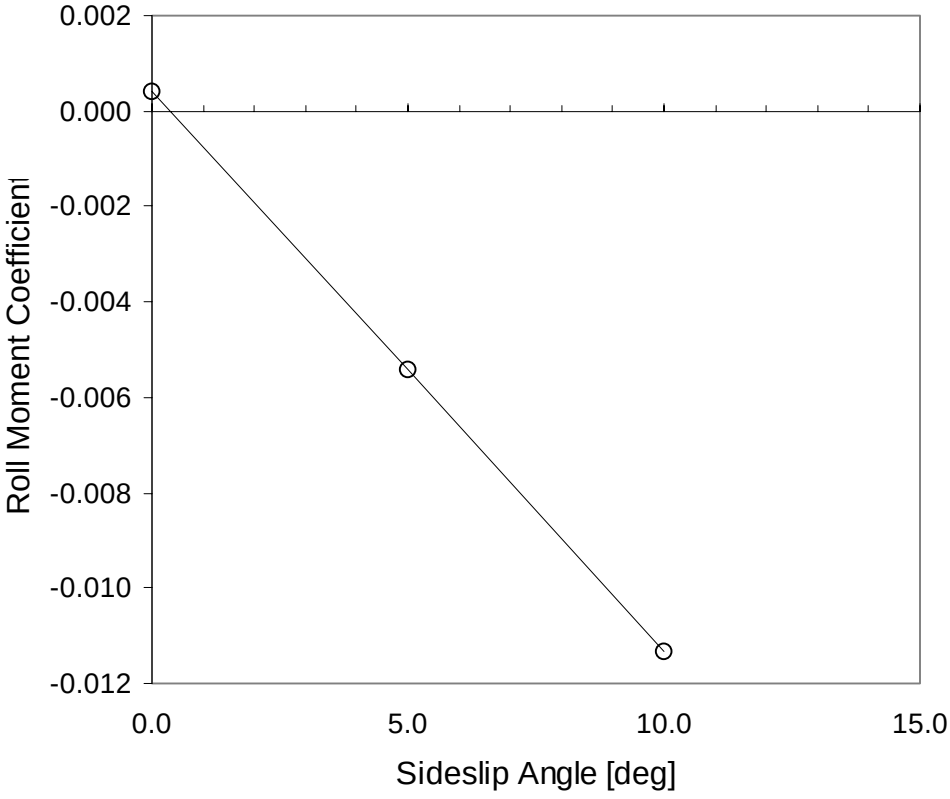

Figure 4: Roll Moment Coefficient versus Sideslip Angle

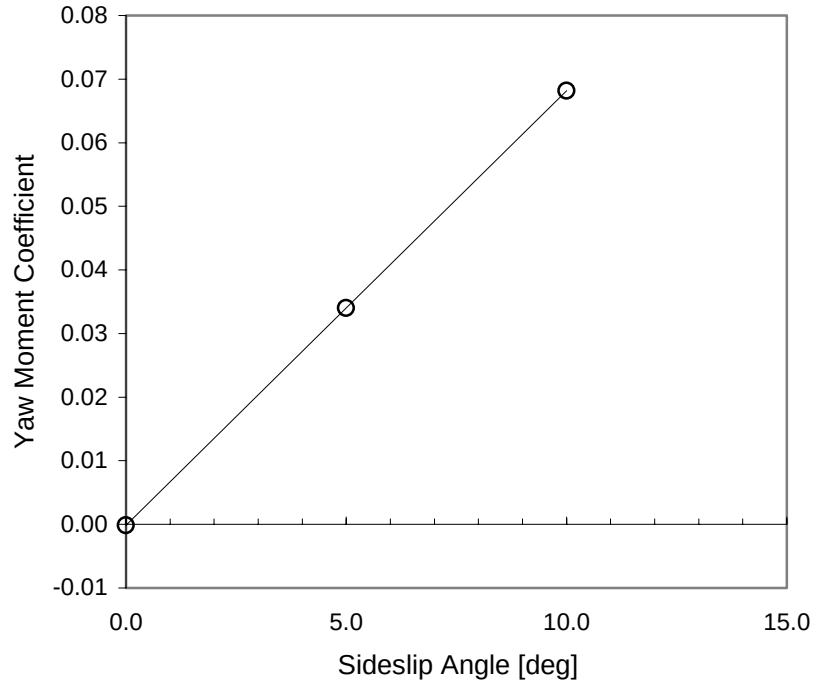

Figure 5: Yaw Moment Coefficient versus Sideslip Angle

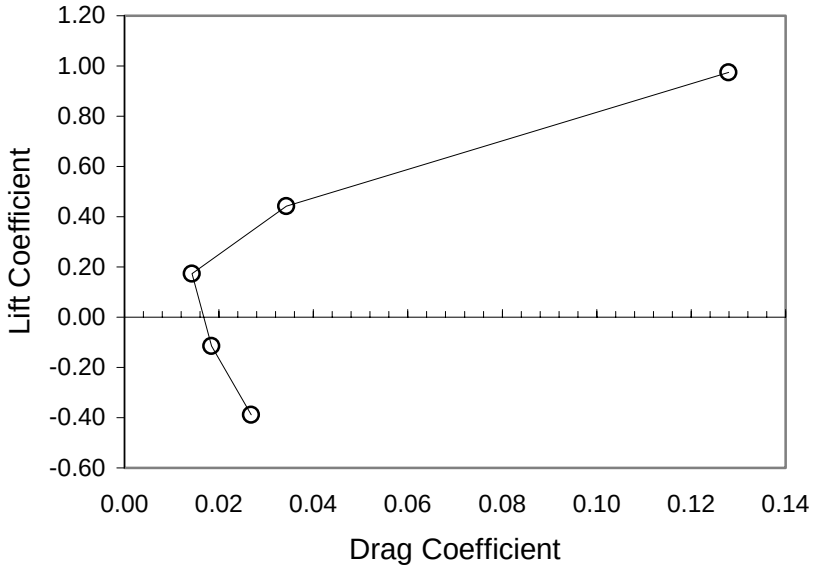

Figure 6: Polar Plot of GMA

Appendix F:
GMA curves

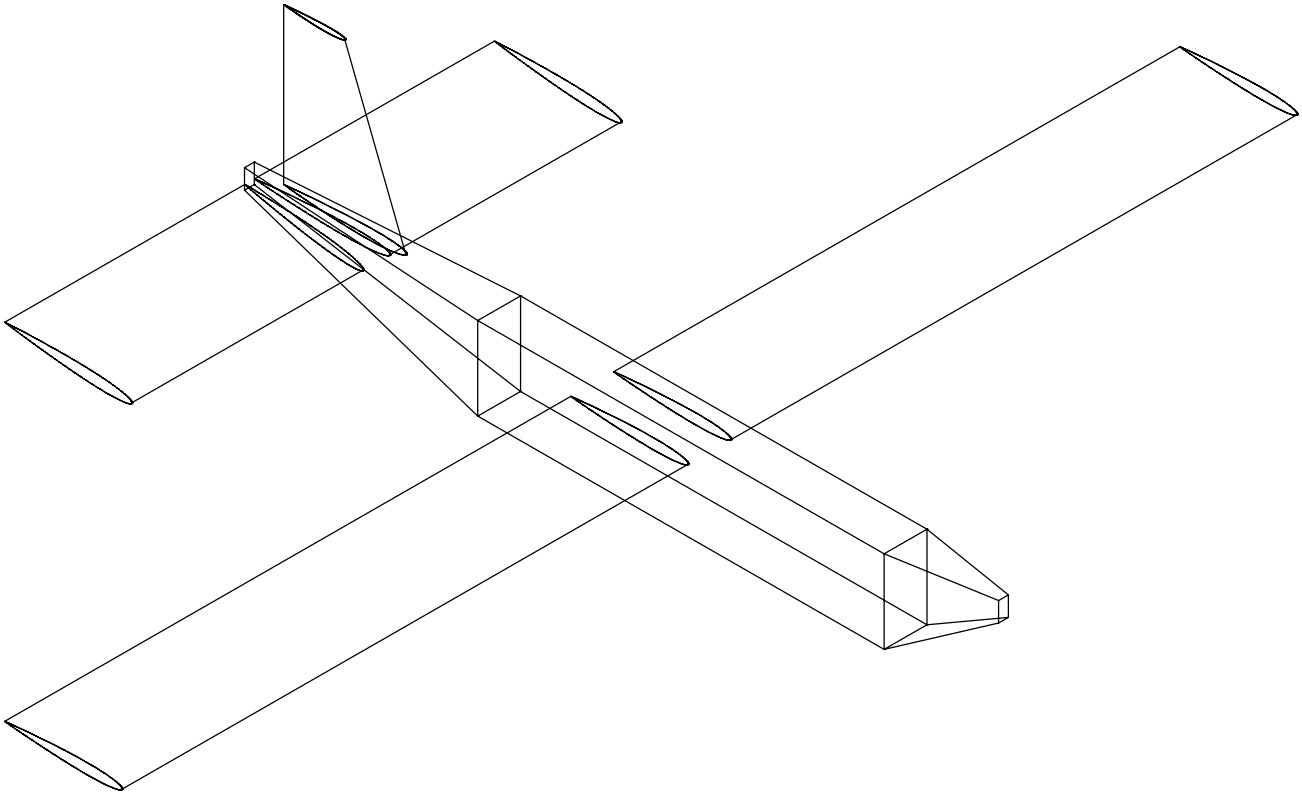

Figure 1. Curve definitions of the GMA

Appendix G:
GMA Pressure Pictures

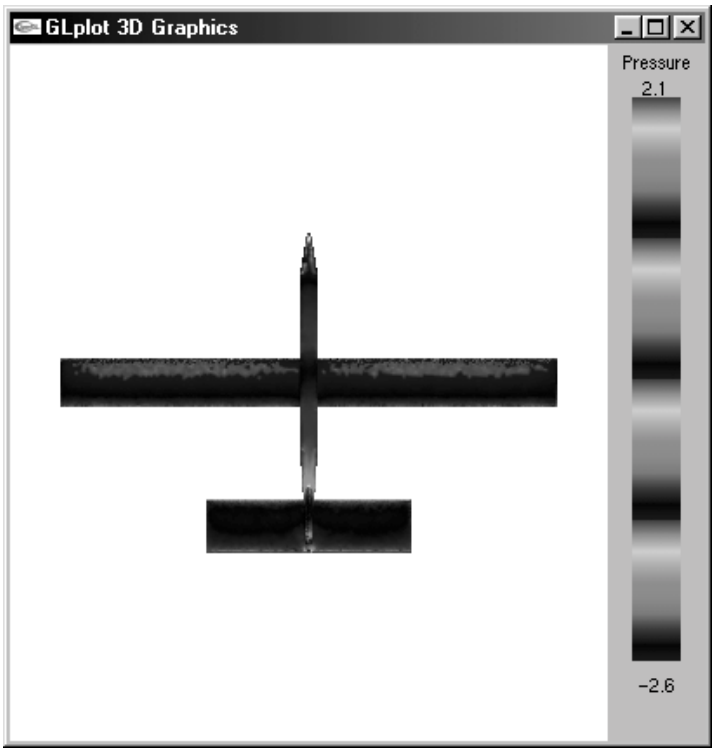

Figure 1: Upper Surface Pressure Plot α=0 β=0

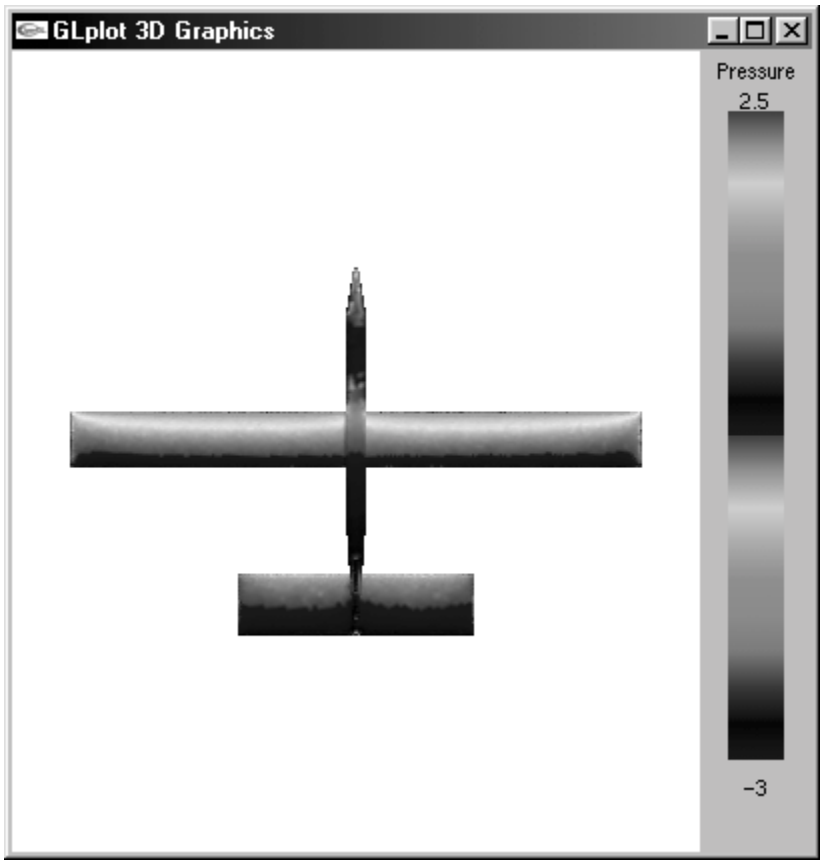

Figure 2: Upper Surface Pressure Distribution α=10 β=0

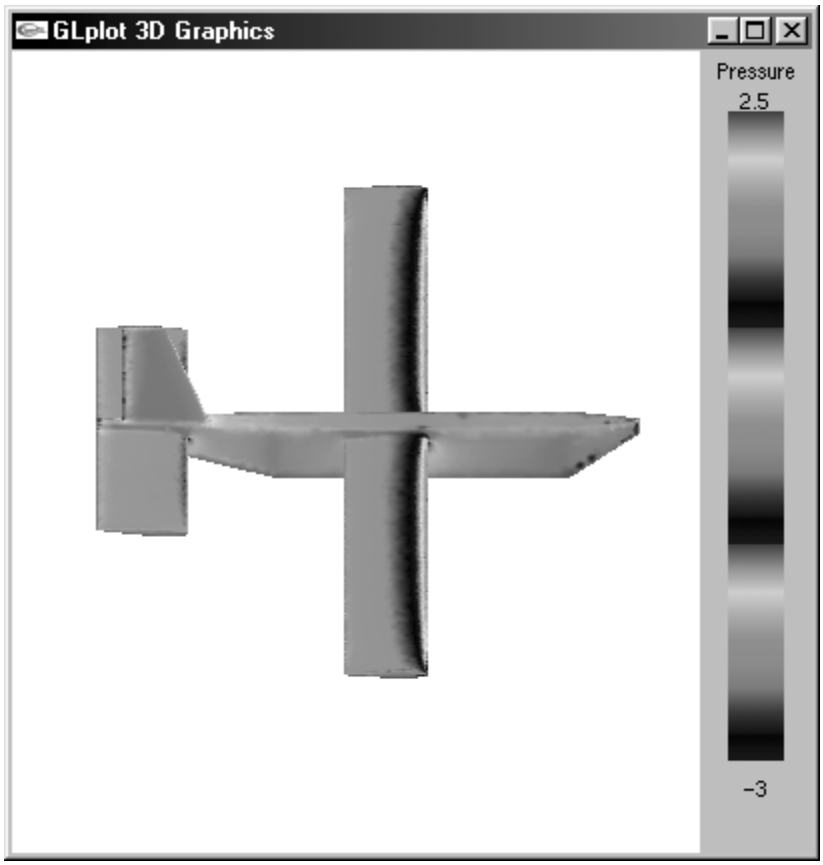

Figure 3: Upper Surface Pressure Distribution α=10 β=0